Biosensors and Bioelectronics 195 (2022) 113664

Contents lists available at ScienceDirect

Biosensors and Bioelectronics

journal homepage: www.elsevier.com/locate/bios

Sensitive and robust chemical detection using an olfactory brain-computer interface

Erez Shor [a,1], Pedro Herrero-Vidal [a,b,1], Adam Dewan [c,d], Ilke Uguz [e], Vincenzo F. Curto [f], George G. Malliaras [f], Cristina Savin [a,b,g], Thomas Bozza [c], Dmitry Rinberg [a,b,h,*]

[a] Neuroscience Institute, New York University Langone Health, New York, NY, 10016, USA
[b] Center for Neural Science, New York University, New York, NY, 10003, USA
[c] Department of Neurobiology, Northwestern University, Evanston, IL, 60208, USA
[d] Department of Psychology, Florida State University, Tallahassee, FL, 32306, USA
[e] Electrical Engineering, Columbia University, 5798 New York, NY, 10027, USA
[f] Division of Electrical Engineering, Department of Engineering, Cambridge University, Cambridge, UK
[g] Center for Data Science, New York University, New York, NY, 10003, USA
[h] Department of Physics, New York University, New York, NY 10003, USA

ARTICLE INFO

Keywords:
Mouse olfaction
Brain-computer interface (BMIs)
Chemical sensing
Neural engineering
Neural signals
Pattern recognition

ABSTRACT

When it comes to detecting volatile chemicals, biological olfactory systems far outperform all artificial chemical detection devices in their versatility, speed, and specificity. Consequently, the use of trained animals for chemical detection in security, defense, healthcare, agriculture, and other applications has grown astronomically. However, the use of animals in this capacity requires extensive training and behavior-based communication. Here we propose an alternative strategy, a bio-electronic nose, that capitalizes on the superior capability of the mammalian olfactory system, but bypasses behavioral output by reading olfactory information directly from the brain. We engineered a brain-computer interface that captures neuronal signals from an early stage of olfactory processing in awake mice combined with machine learning techniques to form a sensitive and selective chemical detector. We chronically implanted a grid electrode array on the surface of the mouse olfactory bulb and systematically recorded responses to a large battery of odorants and odorant mixtures across a wide range of concentrations. The bio-electronic nose has a comparable sensitivity to the trained animal and can detect odors on a variable background. We also introduce a novel genetic engineering approach that modifies the relative abundance of particular olfactory receptors in order to improve the sensitivity of our bio-electronic nose for specific chemical targets. Our recordings were stable over months, providing evidence for robust and stable decoding over time. The system also works in freely moving animals, allowing chemical detection to occur in real-world environments. Our bio-electronic nose outperforms current methods in terms of its stability, specificity, and versatility, setting a new standard for chemical detection.

1. Introduction

In the last few decades, significant effort has been dedicated to developing artificial detectors for volatile organic components, the majority of which use mass spectroscopy (Dung et al., 2018) or nano-technology (Nakhleh et al., 2017) approaches. However, the best chemical detectors to date emerged through biological evolution. An animal nose outperforms most artificial detectors in terms of its versatility, speed, and sensitivity to specific volatile chemicals. This has resulted in an increased use of animals in chemical detection applications such as homeland security, defense (Bonfanti, 2014), healthcare (Bomers et al., 2012; Seo et al., 2018), agriculture and other fields of human activities (Dung et al., 2018). Since the first (to the best of our knowledge) systematic training of dogs for human tracking purposes in 1899 (Bailey, 1995), animals have been employed to locate a wide variety of chemical signatures including explosives (Kranz et al., 2014), illegal substances (Jezierski et al., 2014), bed bugs (Cooper et al., 2014), and electronics (DeGreeff et al., 2017), as well as to diagnose diseases

* Corresponding author. Neuroscience Institute, New York University Langone Health, New York, NY, 10016, USA.
E-mail address: rinberg@nyu.edu (D. Rinberg).
[1] Equal contribution.

https://doi.org/10.1016/j.bios.2021.113664
Received 13 April 2021; Received in revised form 9 August 2021; Accepted 20 September 2021
Available online 28 September 2021

such as tuberculosis (Ellis et al., 2017), cancer (Nardi-Agmon and Peled, 2017; Seo et al., 2018) and Parkinson's (Trivedi et al., 2019). Despite the challenges and expenses associated with training (Weiss, 2002), chemical detection by animals remains the gold standard in the field.

One significant limitation to using animals for chemical detection is the necessity of training. Training is arduous and expensive, and is usually limited to a binary reporting of the presence of only one chemical or group of chemicals (Bonfanti, 2014). Alternatively, recording electrophysiological responses from the intact olfactory system, eliminates the necessity of training and is not limited to specific odorants. Such a bio-electronic nose (BEN) would retain the benefits of the biological system but circumvent the difficulties in measuring chemical detection behaviorally. The success of this approach would be dependent upon reliably interfacing electronics with the olfactory system in animals and interpreting the resulting signals, both represent significant engineering challenges.

The early mammalian olfactory system has most of the properties required by any chemical detector. The geometry of the nose and sniffing behavior has solved the non-trivial problem of fast (~100 ms), reliable delivery/removal of odorants to the chemical detectors. These volatile odorants bind to a subset of ~1200 olfactory receptor (OR) types, each monoallelically expressed within population of olfactory sensory neurons in the olfactory epithelium (Buck and Axel, 1991). The existence of a large number of different ORs ensures high sensitivity to a broad range of different chemicals. All olfactory sensory neurons (OSNs) that express the same receptor converge onto structures called glomeruli, which are arranged on the surface of the olfactory bulb. These glomeruli integrate the signals from a large number of functionally identical sensors, maximizing the signal-to-noise ratio. Importantly, the representation of chemical information at this level is robust to animal learning or internal state. And lastly, modern genetic methods in mice allow for modification the repertoire of olfactory receptor genes and the arrangement of glomeruli to potentially tune the system for specific tasks. Thus, the olfactory bulb is a seemingly ideal and convenient location to readout the chemical information by brain-computer interface.

Here we report the development of a novel BEN based on multi-site electrophysiological recording from the mouse olfactory bulb. Our BEN remained stable over multiple months and was able to detect and correctly identify odorants at concentrations comparable with the behavioral sensitivity of trained animals, even in the presence of a background odor. Further, the BEN is applicable to real-world scenarios as it could be successfully employed in freely moving mice. To investigate a mechanism to enhance BEN detection capabilities for specific odorants, we tested transgenic mice in which a specific receptor type was overexpressed. In this case, the BEN displayed improved detection in the presence of masking odors, without affecting overall sensitivity. These results highlight the potential of our original application-ready BEN systems for advanced chemical detection.

2. Results

2.1. Basic characterization of the odor related signals

Our overall BEN design is schematized in Fig. 1A. We measured odor-driven spatiotemporal patterns of odor-evoked neuronal activity, by chronically implanting mice ($n = 18$) with a 64-site surface electrode array positioned on the dorsal surface of the olfactory bulb. We recorded local field potentials (LFP) from the surface of the bulb in awake, head-fixed mice during the presentation of both monomolecular odorants and odorant mixtures at different concentrations. To monitor the delivery of odors to the nasal cavity, we recorded sniffing patterns via an external pressure sensor located in the odor port. All stimuli induced odor responses which vary across individual electrode sites (Fig. 1B).

To demonstrate the site-specific sensitivity of our recording method, we selectively stimulated a single glomerulus using optogenetic approach (Smear et al., 2013). We used a strain of mice (M72S50-ChR2) in which OSNs expressing a specific receptor (M72) also expressed ChannelRhodopsin2 (ChR2) and thus can be activated by light. We activated a single M72 glomerulus by shining light on the axons of M72 OSNs and recorded signals from an electrode array which covered this glomerulus. We observed that only the few electrode sites that were in close proximity to the activated glomerulus elicited a transient light-evoked response (Fig. 1C). These data show that activation of individual glomeruli elicits a detectable and spatially localized signal.

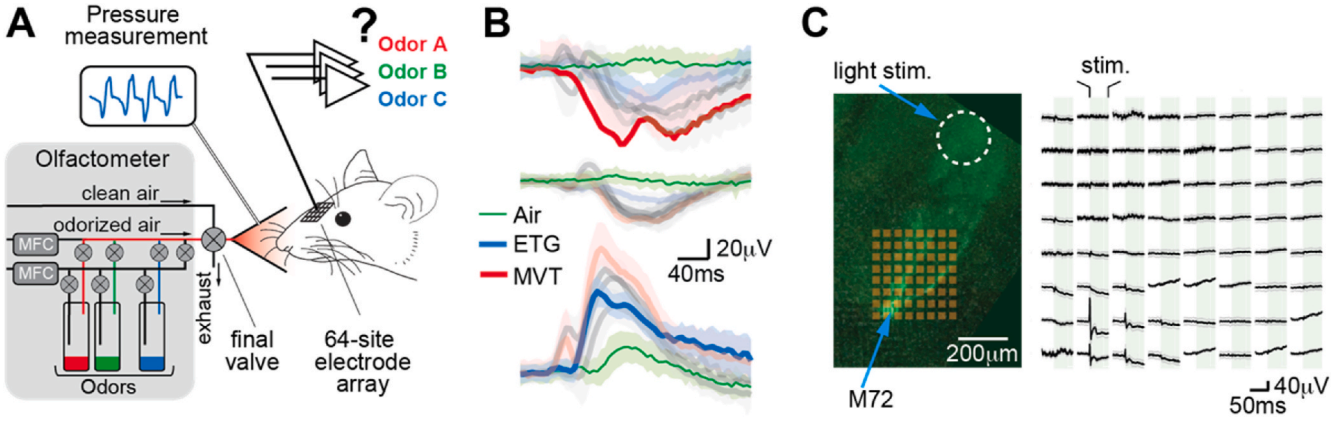

Fig. 1. Bio-electronic nose design and input signal characterization. **A.** BEN design schematic. A mouse is exposed to various odors at different concentrations delivered from an odor port using an air-dilution olfactometer that regulates flow rates with mass flow controllers (MFCs). The sniff pattern is monitored by a pressure sensor in the odor port. A grid electrode with 64-sites is chronically implanted on the mouse olfactory bulb. The odor-evoked neural responses captured by the system are then used to extract odor information. **B.** Example responses from representative electrodes for ethyl tiglate (ETG, blue), methyl valerate (MVT, red), and air (green). Shaded areas indicate standard deviation (s.d.) across trials. **C.** *Left:* Image of the olfactory bulb with a single M72 glomerulus expressing ChR2 and YFP (axons and glomerulus in bright green), with a grid electrode array positioned on the surface of the bulb. The small squares are individual electrode sites. The circle indicates the position of the light spot for illumination of the OSNs axons converging on the photoactivatable glomerulus. *Right:* Site-specific signals in response to light stimulation across the entire electrode array. Black traces represent the average response, gray lines show standard deviation (s.d.) (n = 26 trials). The green shaded area indicates stimulus presentation. (For interpretation of the references to color in this figure legend, the reader is referred to the Web version of this article.)

2.2. BEN accurately and rapidly classifies odor identity

To determine whether signals from the olfactory bulb could be used to identify specific chemicals, we stimulated the BEN ($n = 6$) with a set of individual odorants—methyl valerate (MVT), ethyl tiglate (ETG), hexanal (HEX), carvone (CAR), and benzaldehyde (BZD). The odorant set included chemicals form the same (ETG and MVT) and different groups (CAR and MVT), and those which activate predominantly dorsal (MVT and BZD) and ventral (CAR) glomeruli.

We developed a robust and sensitive odor decoder by extracting the different spatiotemporal features from the odor-evoked signal transients (Fig. 1B). We applied dimensionality reduction methods on the signals, as the neural representation of odors is thought to be low-dimensional (Laurent, 2002; Bathellier et al., 2008). This resulted in a representation of odor responses as well separated trajectories in neural space. Visualization of the trajectories in a three-dimensional space showed that odor classes are well separated within the first sniff cycle (~300 ms) (Fig. 2A). To define the subset of odor informative dimensions of this odor space, we decoded odor identity using increasing numbers of principal components (PCs), ordered according to the relative variance explained. We observed that the classification performance for 6 odor-label task plateaus after the first five PCs, which explained on average 87% of the variance (Suppl. Fig. 1A).

Thus far, our analyses have included data for the whole sniff cycle (0–300 ms after inhalation onset). To validate the choice of this time interval and further characterize the information content of the temporal responses, we first assess the performance of the classifier when we provided it with incremental fractions of the temporal sequence. The classification accuracy given our selected features, plateaus within 300 ms after inhalation onset (Fig. 2B, Suppl. Fig. 1B). If we instead use a 30-ms sliding window for classification, we observed that most of the odor identity information is present between 40 ms and 150 ms after inhalation onset (Suppl. Fig. 1C). Overall, these results show that we can detect chemical identity both rapidly and reliably.

Results from our designed classifier on a 6 odor-label task shows that we can correctly identify the different odors with little error across chemical classes (Fig. 2C). Our BEN provided up to 97% classification accuracy for the animal with the best performance and an average accuracy of 83.4% for the entire cohort (Fig. 2D and Suppl. Fig. 1D–F).

2.3. BEN performance is robust and stable over time

Stable long-term recordings are critical for any BEN in order to maximize their efficiency and minimize any costs associated with the surgeries, additional animals, and the time needed to collect training data for the decoder. To assess the stability of our device, we tested whether the BEN ($n = 6$) could reliably decode odor identity at different time points after electrode implantation. We found that odor specific responses were precise and stereotypic over a long period of time (Fig. 3A). Decoding the chemical identity from sessions recorded days or even as long as 6 months after implantation, resulted in cross-validated classification performance over 65% accuracy in all cases and, in most cases, well over 80% accuracy. Note that we didn't observe significant reduction in performance even at the longest time tested, six months

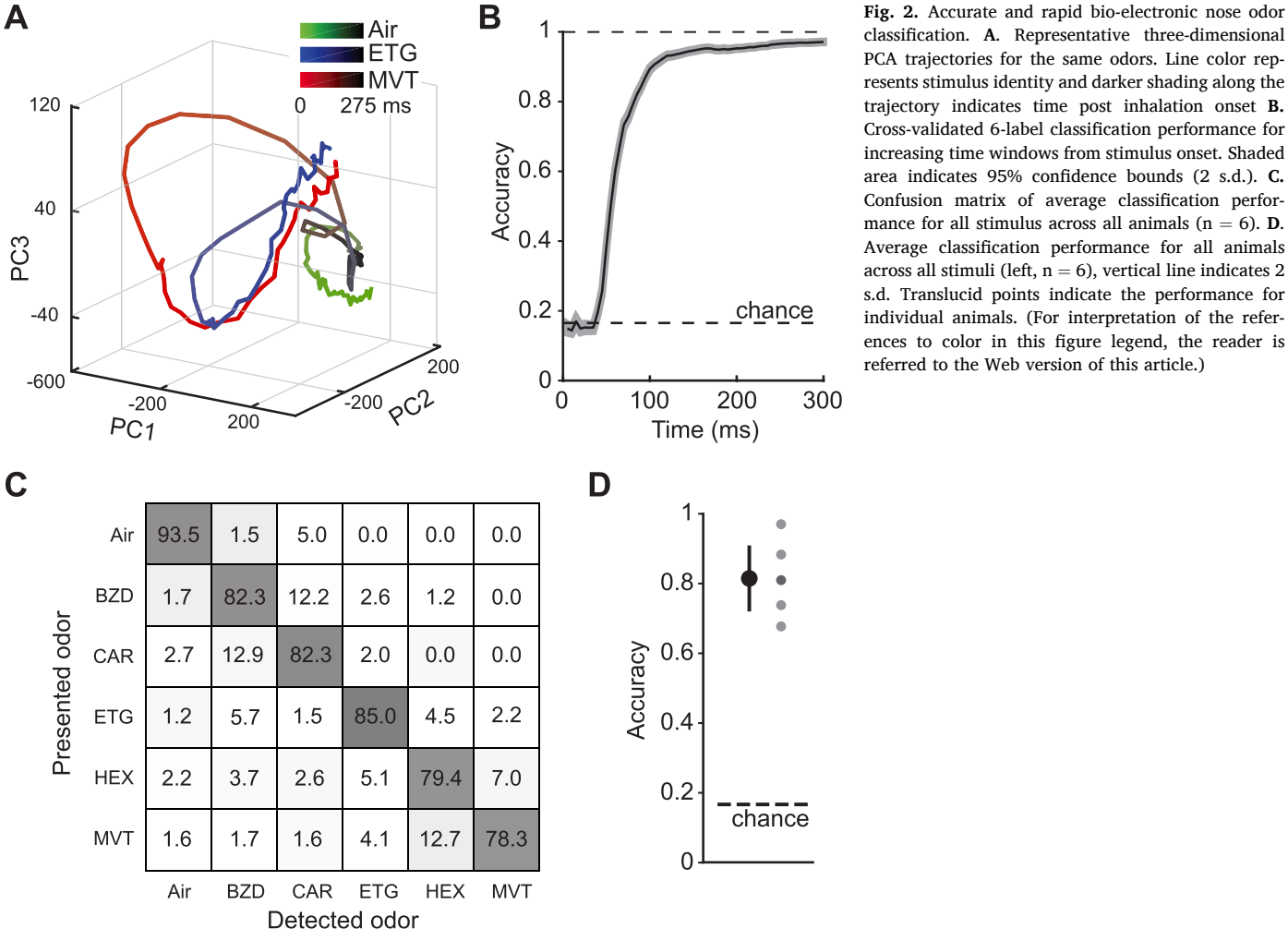

Fig. 2. Accurate and rapid bio-electronic nose odor classification. **A.** Representative three-dimensional PCA trajectories for the same odors. Line color represents stimulus identity and darker shading along the trajectory indicates time post inhalation onset **B.** Cross-validated 6-label classification performance for increasing time windows from stimulus onset. Shaded area indicates 95% confidence bounds (2 s.d.). **C.** Confusion matrix of average classification performance for all stimulus across all animals (n = 6). **D.** Average classification performance for all animals across all stimuli (left, n = 6), vertical line indicates 2 s.d. Translucid points indicate the performance for individual animals. (For interpretation of the references to color in this figure legend, the reader is referred to the Web version of this article.)

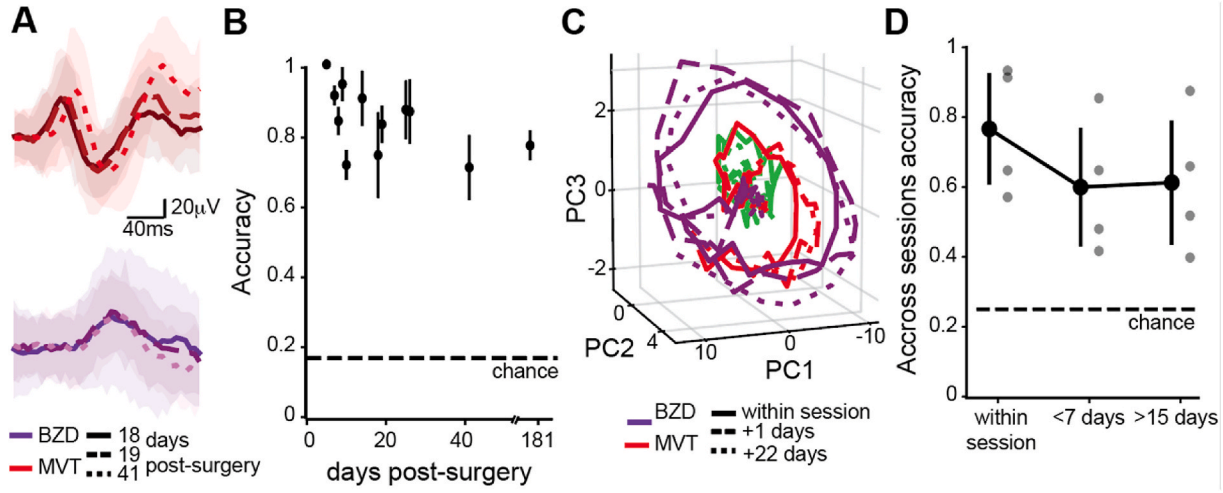

Fig. 3. Odor identification across extended time intervals. **A.** Representative traces for representative electrodes in response to MVT (red) and BZD (purple) for the same animal at different times post implantation: 18 days solid line, 19 days – long dashed line, 41 days – short dashed line. Shaded areas indicate 95% confidence intervals (2 s.d.). **B.** Average cross-validated classification accuracy in a 6-label task for different recording sessions ($n = 12$) and animals ($n = 6$), at different times post electrode implantation (vertical lines indicate 2 s.d.). **C.** Example animal 3-D trajectories in the same PCA space aligned to the first session for air (green), BZD (purple) and MVT (red). The different line styles indicate the session that the trajectories come from. **D.** Classification performance in a 4-label classification task across sessions. Results for the first session are cross validated performance, within session. Results for sessions recorded within seven days of the first session or over fifteen days after test generalization performance of the classifier trained on the first session. Large dots indicate average performance, vertical lines 2 s.d., and translucid dots indicate individual animal averages ($n = 4$). (For interpretation of the references to color in this figure legend, the reader is referred to the Web version of this article.)

post-surgery (Fig. 3B).

To assess the robustness of BEN performance, we tested in $n = 4$ animals whether previously acquired data could be used to predict odor identity in a later session. We used data that met two conditions: 1) recordings from animals that were presented with same odorants in at least three sessions and 2) the sessions occurred over at least a three-week window with the first two sessions occurring in the first week and last session occurring two weeks later. In order to decode across sessions, we developed a two-step strategy. First, we estimated the low-dimensional PCA space and trained the linear SVM decoder exclusively using data from the first session. Second, we tested the ability of the trained decoder to predict stimulus identity by aligning the responses of the later sessions within the PCA space. Visual inspection of the average trajectories in the shared-PCA space showed clustering among stimuli across the different sessions (Fig. 3C). The across-session classification performance was 61% and stable for all recordings (Fig. 3D). Together, our BEN provides reliable stimulus identification over time and stable recordings at least half a year after implantation.

2.4. Detection accuracy matches behavioral thresholds

Odors are usually presented at different and unknown concentrations. Can the BEN predict odor concentration, and what is the concentration range of odor detection? To answer these questions, in $n = 8$ animals we recorded neural signals in response to single odorants presented across a wide range of odorant concentrations. We observed that changes in odorant concentration resulted in a qualitative scaling of the signal, with higher concentrations resulting in a larger signal amplitude and shorter response latency (Fig. 4A and Suppl. Fig, 2). Using the previously identified spatiotemporal features of the responses to predict the concentration via linear regression we were able to predict the odorant concentration across several orders of magnitude change with minimal error (~1.1 log10 M units) (Fig. 4B; for concentration classification see Suppl. Fig. 3A). In fact, this BEN was able to reliably measure MVT concentration as low as $\sim 10^{-16}$ M. Given this extraordinary sensitivity, we next tested whether the limits of BEN sensitivity matched the behavioral threshold of the animal. To define the relative sensitivity of the BEN, we trained the classifier to discriminate between an odorant at any non-zero concentration versus air, using the same data as for concentration classification analysis. This data was compared to the behavioral detection thresholds measured in animals using a go/no-go thresholding paradigm (Dewan et al., 2018). Two odorants were tested: MVT, an ester that generates broad patterns of activity in the olfactory bulb, and PEA, an amine that specifically activates a small subset of dorsal glomeruli (Dewan et al., 2018). For both odorants, the classification accuracy of the BEN performed well with high concentrations and dropped to chance at the lowest concentration tested. We found that the detection accuracy of this BEN was very similar to the sensitivity of the animal (Fig. 4C; behavioral data from (Dewan et al., 2018); $n = 8$). We quantified behavioral and BEN sensitivity as the concentration at half maximal performance, EC_{50}. For MVT, the sensitivity of the BEN ($EC_{50\_BEN} = 4.8 \pm 0.3 \times 10^{-12}$ M, mean ± SD) closely matched that for the behavioral performance (sensitivity = 1.7×10^{-12} M (Dewan et al., 2018)). For PEA, the sensitivity ($EC_{50\_BEN} = 3.1 \pm 0.2 \times 10^{-11}$ M) was within one order of magnitude of the behavioral threshold (sensitivity = 5.0×10^{-12} M (Dewan et al., 2018)) (Fig. 4C). These results show that our BEN detection performance rivals the capabilities of trained animals.

3. Detection accuracy persists in the presence of background odor

Under natural conditions, monomolecular odors are rarely present in isolation. To test the BEN under more realistic conditions, we measured the detection accuracy of the same two odorants as mixtures, to mimic a target odor masked by a background.

First, we tested the sensitivity of the BEN to MVT masked with two concentrations of PEA (Low: 4.4×10^{-10} M and High: 4.4×10^{-8} M; Fig. 4D left; $n = 5$). The sensitivity and odor identification accuracy of the BEN was compared in both the presence and absence of the masking odor (i.e., PEA). We observed that as the concentration of masking odor increased, the sensitivity of the BEN decreased ($EC_{50} = 4.8 \pm 0.3 \times 10^{-12}$ M for no mask, to $6.6 \pm 0.3 \times 10^{-11}$ M for the low concentration mask, and $7.6 \pm 0.1 \times 10^{-11}$ M for the high concentration mask). However, the odor identification accuracy of the BEN did not differ according to the concentration of the background odor (accuracy = 90

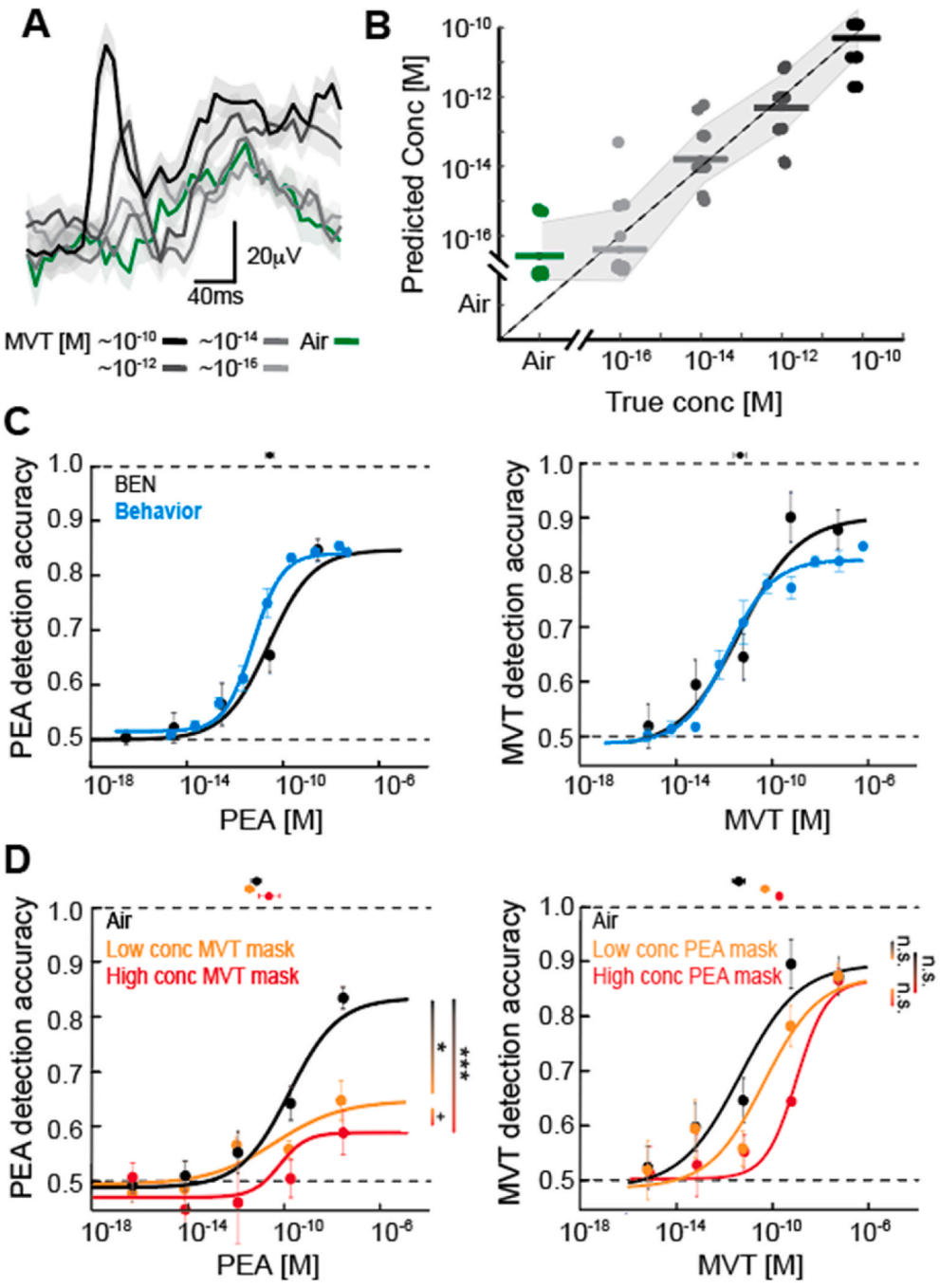

Fig. 4. BEN concentration performance and sensitivity to background odors. **A.** Average signal of a representative electrode site for different concentrations of MVT and air (n = 20 trials per concentration). Shaded areas indicate standard error of the mean (s.e.m.). **B.** Comparison of BEN concentration estimates (linear regression) to true concentration, horizontal bars and dots indicate averaged and individual animal predictions, shaded area corresponds to ±1 s.d. (n = 8). **C.** Average accuracy for mouse behavioral performance in odor detection task as a function of odor concentration (blue, n = 8) for two odors PEA (left) and MVT (right), and BEN performance in the same conditions (black, n = 10). Lines are model fits (see Methods). Maximum behavioral performance is limited to 85%. **D.** BEN average odor detection accuracy in the presence of a masking odor (n = 5) for detection of PEA in the presence of MVT (left) and detection of MVT in the presence of PEA (right), without a mask (black), and for low (orange) and high (red) mask concentrations. EC50 values are indicated as dots with error bars above each plot in C and D. Vertical lines in D indicate two-tailed *t*-test comparison between conditions (n.s. $p > 0.1$, + $p < 0.1$, *$p < 0.05$, ***$p < 0.001$). (For interpretation of the references to color in this figure legend, the reader is referred to the Web version of this article.)

± 9% for no mask, 89 ± 8% for high concentration PEA mask, and 89 ± 12% for low concentration PEA mask, comparison between no mask and low/high concentration mask: $p \sim 0.48/0.50$, two-tailed *t*-test). In contrast, the sensitivity of the BEN to PEA in the presence of two concentrations of MVT (Low: 7×10^{-10} M and High: 7×10^{-8} M) did not differ ($EC_{50} = 3.1 \pm 0.2 \times 10^{-11}$ M for no mask, $1.3 \pm 0.4 \times 10^{-11}$ M for low concentration mask, and $4.8 \pm 0.4 \times 10^{-11}$ M for high concentration mask; Fig. 4D right; $n = 5$). However, the odor identification accuracy of the BEN decreased with higher masking concentrations (no mask: 85 ± 3%; low conc. mask: 65 ± 4%; high conc. mask: 60 ± 9%; $p < 0.02/0.0002$, two-tailed *t*-test) (Fig. 4D). It is possible that this odor-specific difference relates to the patterns of glomerular activation elicited by the two odorants (see Discussion). Overall, the data show that the BEN can reliably detect and classify a target odor in a mixture, even when masked by a background odorant presented at a high concentration and presumably activating a large plurality of glomeruli —a step towards real-world applications.

3.1. *BEN target detection accuracy improvement via receptor overexpression*

One of the unique features of a mouse-based BEN is the ability to genetically modify the relative abundance of specific OSN subtypes in the olfactory epithelium, which could presumably tune the system to specific odorants. We hypothesized that increasing the number of glomeruli corresponding to this receptor (TAAR4) might improve the detection of PEA, while not changing the detection of MVT (to which TAAR4 does not respond). To begin exploring this capability, we tested the effect of increasing the number of OSNs (and glomeruli) that express the PEA threshold-determining receptor (TAAR4) (Dewan et al., 2018)

on BEN detection accuracy. The TAAR4 over-expressing (OE) mouse strain significantly increases the abundance of TAAR4 OSNs (12x) and glomeruli (7x) (Dewan et al., 2018) (Fig. 5A). We compared the BEN performance for wild-type (WT) and TAAR4 over-expressing (OE) animals ($n = 4$) for detection of PEA and MVT, with and without masking (see above).

The over-expression of TAAR4 significantly improved PEA detection accuracy in both the presence and absence of a masking odor. In the absence of a mask, OE mice had a higher detection accuracy (92 ± 8%) for this odor than WT mice (85 ± 3%; $p < 0.01$). Similarly, presence of a masking odor, OE mice also had a higher detection accuracy (low: 82 ± 16%; high: 70 ± 12%) for this odor than WT mice (low: 65 ± 4%; high: 60 ± 9% ($p < 0.02$) (Fig. 5B left, Suppl. Fig. 3B). However, this genetic manipulation did not influence the sensitivity of the BEN (EC_{50} values were comparable at $5.4 \pm 0.1 \times 10^{-11}$ M, $1.2 \pm 0.1 \times 10^{-11}$ M and $1.58 \pm 0.2 \times 10^{-11}$ M for no mask, low and high concentration masks respectively).

As predicted, the over-expression of TAAR4 did not significantly improve the maximum detection accuracy for MVT. Specifically, in the absence of a mask, OE mice (92 ± 3%) and WT mice had similar maximum accuracies (90 ± 9%; $p = 0.08$). Similarly, in the presence of a masking odor, OE mice (low: 90 ± 2%; high: 89 ± 7%) have similar maximum detection accuracy values as WT mice (low: 89 ± 8%: high: 89 ± 12%; $p > 0.31$). Interestingly, the sensitivity of the BEN for MVT decreased for OE mice ($2.0 \pm 0.1 \times 10^{-11}$ M) as compared to WT mice ($4.8 \pm 0.4 \times 10^{-12}$ M) in the absence of a masking odor. In the presence of low conc. masking odor, the effect was weaker with OE mice ($7.6 \pm 0.1 \times 10^{-11}$ M) being approximately one order of magnitude less sensitive than WT mice ($6.6 \pm 0.3 \times 10^{-12}$ M). In the presence of a high concentration masking odor, OE mice ($8.9 \pm 0.1 \times 10^{-10}$ M) were even more similar to WT mice ($4.1 \pm 0.2 \times 10^{-11}$ M). (Statistical comparison between all conditions is presented in Suppl. Fig. 4).

Thus, the overexpression of a threshold-determining receptor improves the overall performance of the BEN, enhancing its sensitivity and maximum accuracy for a specific odorant in both the presence and absence of an odor background.

3.2. Chemical identification in freely moving animals

The applicability and utility of the BEN as a robust chemical detector is also dependent upon its portability. To test chemical identification of the BEN in freely moving animals, we built a pseudo-naturalistic odor landscape with two odor sources, MVT and ETG (Fig. 6A). The odor zone was confined to the ends of the arena using suction and confirmed using a photo-ionization detector (PID) (Fig. 6B). A mouse was allowed to freely move in the arena while being video tracked, and the signals from the implanted electrode array were recorded via flexible cable and synchronized to the video frames for analysis (Suppl. Video 1). This preparation imposes several new challenges for the BEN: 1) sniffing behavior is not externally monitored, 2) the presence and movement of the animal in the arena can introduce contamination and background odors, 3) the odor zones contain a range of concentrations depending on location, 4) animal movement can introduce electrical artifacts, and 5) continuous exposure to a single odor can result in adaptation changes in the neural response, and thus odor responses on an individual sniffs may depend on the previous sniff history.

To address these caveats, we first estimated sniffing behavior from the low frequency components of the response (See Methods, and Suppl. Fig. 5). To account for previous odor exposures, we used a Hidden Markov Model that captures temporal dependencies across sniffs for stimulus identification (see Methods). Despite the limitations, the BEN was able to correctly identify the stimulus odor in this naturalistic environment (Fig. 6C and D). These results provide proof-of-concept evidence supporting the use of our BEN system in real-world chemical sensing.

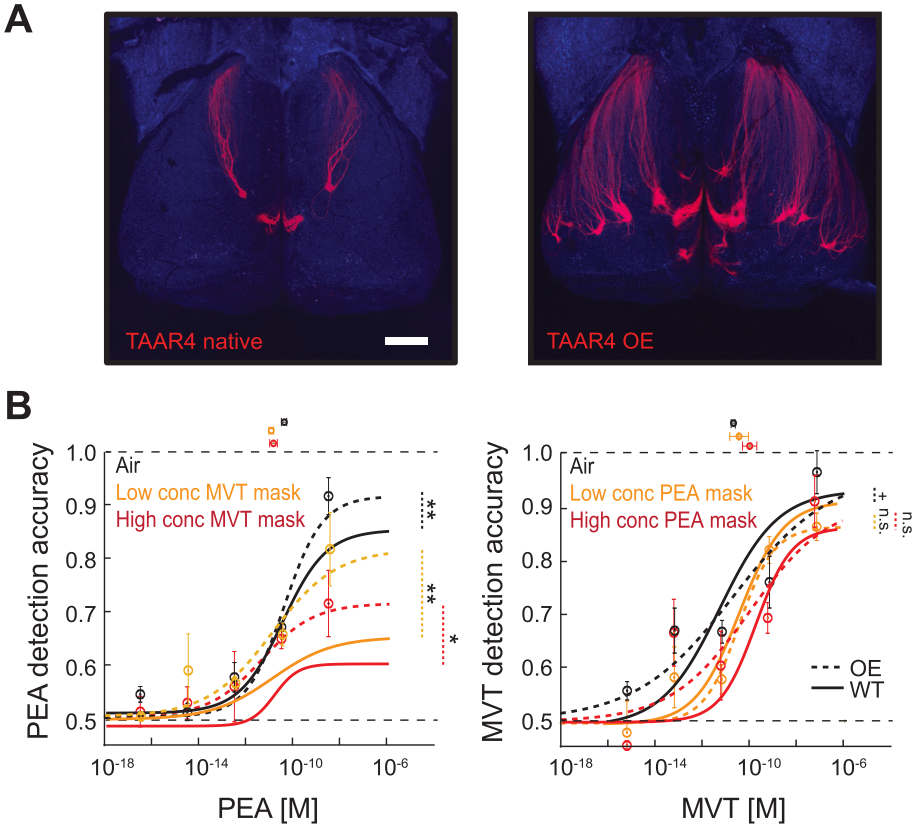

Fig. 5. Genetic overexpression effect on chemical detection. **A.** Fluorescent image of olfactory bulbs of unmodified, native (WT, left) and overexpresser (OE, right) animals. All OSN expressing TAAR4 receptors also expressed RFP. Scale bar = 500 μm **B.** BEN odor detection accuracy in the presence of a masking odor for OE mice ($n = 4$) (circles - average performance, error bars - ±1s.d, dashed lines – model fits) and for WT mice ($n = 4$) (solid line – model fits from Fig. 4D, data points are omittedfor detection of PEA in the presence of MVT (left) and detection of MVT in the presence of PEA (right), without a mask (black), and for low (orange) and high (red) mask concentrations. EC_{50} values are indicated as dots with error bars above each plot. Vertical lines indicate two-tailed *t*-test comparison between WT and OE for all conditions (n.s. $p > 0.1$, + $p < 0.1$, *$p < 0.05$, ***$p < 0.001$). (For interpretation of the references to color in this figure legend, the reader is referred to the Web version of this article.)

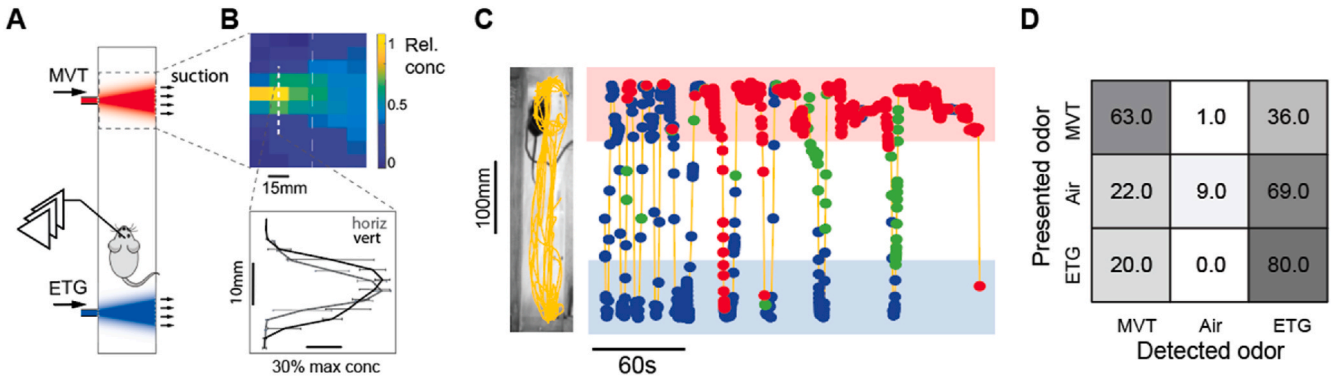

Fig. 6. Bio-electronic nose odor identification in freely moving animals. **A**. Schematic of the experimental design. Animals can move freely in a narrow arena with two odor sources (MVT – red, and ETG – blue), Neural responses are recorded via flexible cable, and animal position is video monitored. **B.** Characterization of the odor landscape. *Top:* Odor concentration distribution in a horizontal plane measured by photo-ionization detector (PID). Odor was presented from a constant airflow source on the left side of the arena and sucked away on the right side of the arena. *Bottom:* A high resolution PID concentration measurement along vertical (black) and horizontal (gray) direction 25 mm from an odor source (white dashed line at the top panel). Error bars are 1 s d. **C.** Example odor classification for individual sniffs (dots) along the arena. The color of the dot indicates the odor detected by Hidden Markov Model (blue ETG, red MVT, green Air), the yellow line indicates the animal trajectory over time and the shaded areas indicate the odorized regions. **D.** Average cross-validated odor classification results for all trials (n = 1241). (For interpretation of the references to color in this figure legend, the reader is referred to the Web version of this article.)

4. Discussion

Here we report a method to exploit the mouse olfactory system for sensitive and versatile chemical detection. Our BEN is capable of discriminating between multiple presented odorants (Figs. 2 and 3), estimating odorant concentration (Fig. 4), and detecting odorants with sensitivities that are comparable with those of well-trained animals (Fig. 4). Moreover, the BEN was able to correctly identify odorants in the presence of background odors – overcoming a significant hurdle for chemical detection. Even in the presence of a high concentration background odor, the BEN performance remained significantly above chance. Beyond its success as a robust chemical detector, the use of mice as a BEN, benefits from the availability of modern genetic tools. The over-expression of a specific OR enhanced sensitivity to the target odor, even in the presence of a background odor, highlighting the flexibility of the BEN to be tuned to specific odorants of interest (Fig. 5). Lastly, the success of this approach in freely moving animals, provides evidence that this BEN can be used for robust chemical detection in naturalistic odor landscapes (Fig. 6).

While our implementation of the BEN requires further optimization, it has shown remarkable performance in initial tests. This performance is notable because it is unlikely that the BEN has direct access to all relevant olfactory sensory inputs. When a trained animal detects a specific odor, the brain has access to information from all olfactory bulb glomeruli. In contrast, the BEN records only some portion of that incoming information, likely the neural activity corresponding to the dorsal glomeruli. It was, therefore, not obvious a priori that the performance of the BEN could rival that of the intact system. Despite this concern, the sensitivity of the BEN was similar to that of behaving animals. Prior work has shown that behavioral detection thresholds are defined by the activation of the most sensitive glomeruli (Dewan et al., 2018). In our experiments, the electrode array was positioned on the OB in a way that most likely covered the glomerulus corresponding to the most sensitive receptor for PEA, TAAR4 (Dewan et al., 2013). This may explain why the BEN was able to detect PEA at such low concentrations.

For MVT, the identity and location of the most sensitive glomerulus is unknown. Even if the most sensitive MVT glomeruli were not covered directly by the array, it is possible that activation of remote glomeruli could create broader perturbations of the LFP, which might then be picked up by underlying electrodes. Such “indirect” detection of signals entering through distant glomeruli could significantly expand the spectrum of chemicals that can be detected at low concentrations and thus its applicability. Similarly, the use of larger electrode arrays, which could cover more glomeruli should further improve BEN detection and discrimination for a large number of odors.

The decoding of chemical information by our BEN was very rapid (~100 ms, Fig. 2B). This time course suggests that early activated glomeruli could play a particularly important role for BEN performance (Carey et al., 2009). We observed that discrimination accuracy for multiple odorants increased as a function of time (Fig. 2F) and saturated quickly (~100 ms), much faster than the activation time course for a majority of glomeruli ((Carey et al., 2009), Fig. 4). The fastest glomeruli to respond may correspond to the most sensitive receptors, which are sufficient to reach high levels of odor discrimination (Wilson et al., 2017).

We also observed that MVT detection is less affected by PEA as a masking odor, compared to PEA detection when using an MVT mask (Fig. 3D). One possible reason for this asymmetry is that MVT may excite a larger number of glomeruli than PEA at the concentrations we tested (McGann et al., 2005; Pirez and Wachowiak, 2008; Dewan et al., 2013; Dewan et al., 2018)). This explanation is also consistent with the fact that when the number of glomeruli activated by PEA is increased via genetic modification, the effect of the MVT mask is suppressed (Fig. 4B&C). These results are crucial for developing future strategies to improve detection of defined odors in the presence of different backgrounds, and underscore the importance of covering a larger number of glomeruli as a pathway towards improving BEN performance.

Real-world chemical detection often requires sampling complex environments (Bonfanti, 2014; Bomers et al., 2012; Seo et al., 2018). While we observed that the BEN can detect chemicals in more naturalistic conditions than well controlled head-fixed setup (Fig. 6), concentration fluctuations, sensory neurons’ adaptation, and the presence of the animals themselves in the environment compromises its performance. Thus, addressing these challenges could further improve BEN detection capabilities in all environmental situations.

In terms of decoding performance, stability and classification capabilities and versatility, our BEN greatly outperformed all previous attempts to use a brain-computer interface to extract chemical information from the early olfactory system of insects or mammals (Dong et al., 2013; Saha et al., 2020). Not only our BEN capabilities surpass other technologies, but they also compare to that of trained animals, while bypassing exhaustive animal training. Additionally, it should be noted that this approach enables the detection of multiple chemicals with a single BEN implanted animal, something not possible for trained animals, which are limited to a binary behavioral output (Leitch et al., 2013).

Overall, our BEN exhibited high accuracy, low latency, robustness and a capability to operate in naturalistic odor environments where target odors are likely to be masked. Tapping into the neural signals yielded a setup that translates odor responses into complex data sets from which we can accurately extract chemical information. This potentially enables us to discriminate a large array of chemical targets using available data science methods. For example, collection of large-scale BEN data of patients' breath, urine or feces odor samples with corresponding medical condition attributes can be used to train a novel diagnosis system. This process could yield the odor footprints of various diseases and provide a cost effective, non-invasive broad-spectrum diagnosis method.

4.1. Materials and methods

4.1.1. Animals

For electrophysiological experiments, we used 11 adult homozygous *M72–IRES-ChR2-YFP* mice (Strain *Olfr160 tm1.1(COP4*/EYFP)Tboz, males*). For experiments with receptor overexpression we used 7 mice that overexpress TAAR4 receptors (5 × 21-TAAR4Tg (Dewan et al., 2018)). For optogenetic stimulation of a single glomerulus we used one male M72/S50-IRES-tauGFP mouse (strain *Olfr545 tm3(Olfr160)Mom*). For behavioral experiments we used C57BL/6 J mice. Animals were 6–10 weeks old at the beginning of experiment and were maintained on a 12-h light/dark cycle (lights on at 8:00 p.m.) in isolated cages in a temperature- and humidity-controlled animal facility. All animal care and experimental procedures were in strict accordance with protocols approved by the New York University Langone Medical Center and Northwestern University Institutional Animal Care and Use Committees.

4.1.2. Chronic electrode implantation

Mice were anesthetized with isoflurane (2–3%) in oxygen and administered ketoprofen (0.1 mg/kg) as analgesic. The animals were secured in a stereotaxic head holder (Kopf). After incision of the scalp the connective tissue covering the skull was removed with H_2O_2 (5%). One micro screw was placed into the skull at 1 mm caudal to lambda. A custom-built plastic 3D-printed head-bar (Osborne and Dudman, 2014) was attached to the skull using Vetbond cyanoacrylate glue. Head-bar and ground screw were cemented in place using dental cement (Dental Cement, Pearson Dental Supply). The skull was thinned and a small craniotomy was performed at the site of the electrode implantation. The surface Electrode (Diagnostic Biochips or Malliaras Lab, Cambridge, UK) then was placed on the bulb. To achieve consistency of placing electrodes across mice, we used M72 fluorescent glomerulus in M72-ChR2 mice as a landmark. For a single glomerulus stimulation experiment, using M72-S50-ChR2 mice we ensure that the electrode covered the fluorescent glomerulus. Following placement, the electrode was secured with Kwik Sil (World Precision Instruments). After the Kwik Sil cured the electrode, PCB was attached to the head bar using 5-min epoxy glue. The electrode surgery site was then sealed with Body double mold rubber (Smooth-On, Easton PA). After surgery, mice were individually housed and given at least two days for recovery before water deprivation or data recording.

4.1.3. Head-fixed experiments

For a majority of experiments, mice were head-fixed with their noses inserted in a Teflon port for odor delivery and sniff recording (read below). Animals were awake and able to freely run on a custom 3-D printed wheel. Prior to data collection, animals were acclimatized to head-fixation in a few short sessions, 15–20 min each.

4.1.4. Odorants

Odorants were obtained from Sigma-Aldrich. CAS numbers, chemical names and concentrations used in each experiment are listed on Table 1. The odorants were diluted in water and kept in dark vials (45 mL volume filed with 5 mL diluted odorant). Dilutions for concentration series (Figs. 3 and 4) were prepared by subsequent dilutions of the freshly made PEA and MVT odorants.

Table 1
Odorants used in the experiments.

Odorant (CAS #)	Abbreviation	Dilution	Headspace concentration
Phenyl-ethylamine (64-04-0)	PEA	2×10^{-2}	4.4×10^{-8} M
		2×10^{-4}	4.4×10^{-10} M
		2×10^{-6}	4.4×10^{-12} M
		2×10^{-8}	4.4×10^{-14} M
		2×10^{-10}	4.4×10^{-16} M
Methyl valerate (624-24-8)	MVT	8×10^{-2}	7×10^{-6} M
		8×10^{-4}	7×10^{-8} M
		8×10^{-6}	7×10^{-10} M
		8×10^{-8}	7×10^{-12} M
		8×10^{-10}	7×10^{-14} M
Carvone (6485-40-1)	CAR	4×10^{-2}	1×10^{-7} M
Ethyl tiglate (5837-78-5)	ETG	3×10^{-2}	1×10^{-6} M
Hexanal (66-25-1)	HEX	1.1×10^{-2}	1×10^{-6} M
Benzal-dehyde (100-52-7)	BZD	8×10^{-2}	1×10^{-7} M

4.1.5. Odor delivery

To deliver odor stimulus for both electrophysiological and behavioral experiments, we used an eight-channel air-dilution olfactometer (Fig. 1A). An olfactometer consisted of two mass flow controllers (MFCs), (Alicat, MC-100SCCM-D/5M/5IN and MC-1SLPM-D/5M/5IN), four inline Teflon four-valve manifolds, (NResearch, 225T082), one on-off clean-air three port bypass valve (NResearch, TI1403270), and eight odor vials. Odors were diluted in water and stored in amber volatile organic analysis vials (Restek, 21797). The total air flow (usually 1000 ml/min) and relative odor concentration were controlled by MFCs. To deliver the odor stimuli, specific odor valves were opened prior to the beginning of each trial and the odorized air flow was diverted to the exhaust line by a final valve (NResearch, SH360T042), while a controlled flow of clean air at the same flow rate was delivered to an odor port. At all times, 1000 ml/min suction was applied near the nose to remove odors and minimize contamination. After flow stabilized (~1 s), the final valve switches between odorized flow and clean air flow, and at the end of stimulus presentation, it switches back to deliver clean air to the odor port. The olfactometer enables the dilution of odors between 10- and 100-fold. Temporal odor kinetics was measured using a mini-PID (Aurora Scientific, model 200 B). The concentration reached a steady state 95–210 ms (depending on a specific odor) after final valve opening. To minimize pressure shocks and provide temporally precise, reproducible, and fast odor delivery, we matched the flow impedances of the odor port and exhaust lines, and the flow rates from the olfactometer and clean air lines. A custom Python code monitored sniff pressure in real time and controlled the opening of the final valve at the onset of exhalation, so that the odor reached steady-state concentration before the next inhalation. Inter-stimulus interval was 7–14 s, during which clean air was flowing through all Teflon tubing.

4.1.6. Sniff recording

To monitor the sniff signal, a sniffing cannula located in the odor port was connected to a pressure sensor through an 8–12 cm long polyethylene tube (801000, A-M Systems). The pressure was transduced with a pressure sensor (24PCEFJ6G, Honeywell) and preamplifier circuit. The signal from the preamplifier was recorded together with electrophysiological data on one of the data acquisition channels.

4.1.7. Optogenetic stimulation

Light stimulation was produced via a 100 μm multimodal fiber coupled to a 473-nm diode laser (model FTEC2471-M75YY0, Blue Sky Research). The end of the fiber was cut flat and polished. The light stimulus power at the open end was measured by a power meter (Model,

PM100D, Thorlabs), and calibrated to adjust the amplitude of the voltage pulses sent to the laser, to achieve a consistent power output across experiments. 10 mW/mm^2 pulses of 1 s duration were used to activate the M72 glomerulus by shining light on the axons outside the electrode (Fig. 1C).

4.1.8. Electrophysiology

A bespoke array of PEDOT:PSS microelectrodes on parylene C was developed for this work using a previously reported fabrication process (Khodagholy, Doublet et al., 2011), with electrodes that had an area of 324 μm^2. Neural signals were recorded using 64 channels digital headstages (Intan RHD-2000, Intan Technologies California, USA) and electrophysiology system (Siegle, Lopez et al., 2017) (Open ephys inc., Massachusetts, USA). Signals were recorded at 2 KHz frequency. The analog sniff pattern signal, and multiple triggers, such as a final valve opening and a beginning of the trail, were synchronously recorded with neural data all as 0–5 V analog signals.

4.2. Data analysis

4.2.1. Preprocessing

Data analysis was performed in Matlab (The MathWorks, Natick, MA) and Python (Python Software Foundation. Python Language Reference, version 3.7.3). A 60 Hz notch filter was applied to all raw signals to remove AC line voltage noise. All signals were low-pass filtered (<100 Hz, 4th order Butterworth filter) and down sampled (10-fold, 200 Hz). Single electrode signals with peaks exceeding 2 mV in a period of 5 s were considered damaged and excluded from the study. An average signal across all electrodes was subtracted from each electrode signals, resulting in both positive and negative stimulus-evoked responses (Fig. 1B). Odor presentation onset was defined as the first time point after the final valve opening when the sniff pressure signal crossed the baseline threshold, indicating inhalation onset.

4.2.2. Dimensionality reduction

To reduce the dimensionality of the 64-channel multi electrode signal, we performed principal component analysis (PCA) on the stimulus-averaged temporal responses. We used 5 PCs based on the variance explained (87% ± 4.6% (s.e.m)) and stimulus decodability (see classification of odor identity methods section).

4.2.3. Classification of odor identity

Decoding of odor identity was performed using a linear support vector machine (SVM; python sklean v. 0.20.3 (Pedregosa et al., 2011)). Feature vectors were built by concatenating 5 PCs projected signals measured in a time window of 300 ms after stimulus onset, discretized in 5 ms bins. To assess stimulus information content an increasing number of PCs were concatenated, in decreasing order of variance explained, using the same time discretization (for Suppl. Fig 2A). To determine information content as a function of the temporal response, in Fig. 2C and Suppl. Fig. 2B additional 5 ms time bins of the 5-PC trajectory were concatenated iteratively up to 300 ms. In Suppl. Fig. 2C a 30 ms window (six 5 ms time bins) of the 5-PCs dynamics were used as features at different times of the odor response. For all results we report cross-validated classification performance (5-fold). We down sampled and bootstrapped (100 repeats) trials to deal with unbalanced group labels. Chance performance was estimated as 1 over the number of classes.

4.2.4. Across sessions odor classification

To decode across sessions, we first constructed the low-dimensional PCA projection as described above using data from the first session for a given animal. Then, we projected the other two sessions using the same loading matrix and aligned the trial-averaged trajectories in PCA space using an orthogonal Procrustes rotation (python scipy 1.2.1). We trained an SVM linear classifier with the above-described features using data from the first session (we reported 5-fold cross-validation accuracy results for this session). We tested generalization performance of the trained classifier in the other two sessions.

4.2.5. Estimation of odor concentration

Estimation of odor concentration was performed using multivariate linear regression, with the same feature vectors described above. We reported 5-fold cross-validation performance.

4.2.6. Calculation of detection accuracy: neural signals

Using the recording for PEA and MVT at five different concentrations (see Table 1), we trained a linear SVM classifier to discriminate odors from air, separately for each concentration (feature vector description in *Classification of odor identity methods section)*. Performance was estimated using 5-fold cross validation. The same procedure was used for discriminating odors vs. air, in the presence of a background odor, at low/high concentration.

4.2.7. Calculation of detection accuracy

The same set of stimuli was used to measure behavioral detection thresholds (see (Dewan et al., 2018) for detailed description). As in the original paper, behavioral performance was fit as:

$$R(x) = R_{min} + \frac{R_{max} - R_{min}}{1 + 10^{n(log_{10}(EC_{50}) - x)}}$$

where x $\log_{10}$ of the concentration, $R_{\min}$ and $R_{\max}$ mark minimal and maximal responses, respectively, EC_{50} is the concentration at half maximal response, and n is the Hill slope. The parameters were estimated using nonlinear regression. The coefficients were estimated using iterative least square estimation (Matlab nlinfit). P-values in Fig. 4 were calculated using two-tailed t-test (Matlab).

4.2.8. Freely moving behavioral experiments

4.2.8.1. Behavioral arena. A long and narrow arena (size $L = 61$ cm, $W = 8$ cm) was built from transparent acrylic sheets (Plaskolite, Colombus, OH). Water delivery to two waterspouts mounted on both ends of the arena was based on gravitational flow controlled by pinch valves (98302–12, Cole-Parmer) connected via Tygon tubing to a stainless-steel cannula (gauge 21, Small Parts capillary tubing), which served as a lick tube. A perpendicular flow of odor connected to the odor delivery system was generated by flowing odor from one side of the arena and mounting an air suction fan on the opposite side.

Odor landscape was measured and calibrated using a photoionization detector (PID) mounted on a micromanipulator. Measurements were taken along the horizontal and vertical axis of the arena with 1 mm intervals. Relative odor concentration was assumed to be directly proportional to the PID readout.

A camera was mounted to obtain a continuous video stream of the arena. The camera video stream was synchronized with the neural data using a digital frame counter recorded simultaneously on video using LED outputs visible on the video frame, and discrete voltage signals recorded by the electrophysiology system.

Water deprived mice were trained to move from side to side of the arena by providing a drop of water every 2 s on each side of the arena.

4.2.9. Sniff estimation for freely moving behavior

We considered that the sniff rhythm is roughly synchronized with ~3 Hz LFP theta rhythm (Suppl. Fig. 4), and extracted the onset of inhalation from the theta-rhythm. The signal from a single electrode site was low-pass filtered (<5 Hz, 4th order Butterworth filter). To obtain the theta component we calculated the morse wavelet transform of the filtered signal and took the maximum component (Lilly, 2017). A reconstructed sniff rhythm was calculated by preserving only the selected frequency and phase, then performing inverse wavelet

transform. Negative zero crossing was identified as inhalation onset. (See Suppl. Fig. 4).

4.2.10. Classification of odor identity in freely moving animals

Decoding odor identity from a naturalistic odor environment comes with a series of limitations. It is important to note that opposite to head-fixed trials that were independent and randomized, there is important temporal structure across trials as well. We used a Hidden Markov Models (HMM) to capture these dependencies, which helped solve caveats such as receptor adaptation, odor contamination or concentration fluctuations. The HMM is determined by emission probabilities for each discrete underlying state (odor label: MVT, Air, ETG) and transition probabilities across these states (assuming Markov or memoryless properties) with gaussian observation noise. We estimated emission and transition properties by expectation-maximization using a subset of sequential trials from the arena where each trial was summarized as average trajectory distance in the 5 PCs space. We used the trained HMM to decode the most likely latent state (odor label) in the held back data set. We reported 5-fold cross-validation performance.

CRediT authorship contribution statement

Erez Shor: Conceptualization, Methodology, Software, Investigation, Writing – original draft, Writing – review & editing. **Pedro Herrero-Vidal:** Methodology, Software, Formal analysis, Investigation, Writing – original draft, Writing – review & editing. **Adam Dewan:** Investigation. **Ilke Uguz:** Resources. **Vincenzo F. Curto:** Resources. **George G. Malliaras:** Resources. **Cristina Savin:** Software, Formal analysis, Writing – review & editing. **Thomas Bozza:** Conceptualization, Methodology, Resources, Writing – original draft, Writing – review & editing. **Dmitry Rinberg:** Conceptualization, Methodology, Writing – original draft, Writing – review & editing, Supervision, Project administration.

Declaration of competing interest

Three authors of the manuscript (Erez Shor, Thomas Bozza and Dmitry Rinberg) are inventors on the patent US2019/027053A1.

Dmitry Rinberg is one of the founders of a company using bioelectronic nose technology.

Acknowledgement

We thank Ezequiel Arneodo and Dion Khodagholy for help at the initial stage of the project, David Godovich, Alexandra Dolzhina, and members of the Rinberg lab for technical help. The project was funded by DARPA grant HR0011-16-0007. PHV was supported by training grant R90DA043849 (NIH). The fabrication of the electrodes was supported by the European Union's Horizon 2020 Research and Innovation Programme under grant agreement No. 732032 (BrainCom).

Appendix A. Supplementary data

Supplementary data to this article can be found online at https://doi.org/10.1016/j.bios.2021.113664.

References

Bailey, W.G., 1995. The Encyclopedia of Police Science. Garland Pub, New York.
Bathellier, B., Buhl, D.L., Accolla, R., Carleton, A., 2008. Dynamic ensemble odor coding in the mammalian olfactory bulb: sensory information at different timescales. Neuron 57 (4), 586–598.
Bomers, M.K., van Agtmael, M.A., Luik, H., van Veen, M.C., Vandenbroucke-Grauls, C. M., Smulders, Y.M., 2012. Using a dog's superior olfactory sensitivity to identify Clostridium difficile in stools and patients: proof of principle study. BMJ 345, e7396.
Bonfanti, M.E., 2014. From sniffer dogs to emerging sniffer devices for airport security: an opportunity to rethink privacy implications? Sci. Eng. Ethics 20 (3), 791–807.
Buck, L., Axel, R., 1991. A novel multigene family may encode odorant receptors: a molecular basis for odor recognition. Cell 65 (1), 175–187.
Carey, R.M., Verhagen, J.V., Wesson, D.W., Pírez, N., Wachowiak, M., 2009. Temporal structure of receptor neuron input to the olfactory bulb imaged in behaving rats. J. Neurophysiol. 101 (2), 1073–1088.
Cooper, R., Wang, C., Singh, N., 2014. Accuracy of trained canines for detecting bed bugs (Hemiptera: cimicidae). J. Econ. Entomol. 107 (6), 2171–2181.
DeGreeff, L.E., Cerreta, M., Rispoli, M., 2017. Feasibility of canine detection of mass storage devices: a study of volatile organic compounds emanating from electronic devices using solid phase microextraction. J. Forensic Sci. 62 (6), 1613–1616.
Dewan, A., Cichy, A., Zhang, J., Miguel, K., Feinstein, P., Rinberg, D., Bozza, T., 2018. Single olfactory receptors set odor detection thresholds. Nat. Commun. 9, 2887.
Dewan, A., Pacifico, R., Zhan, R., Rinberg, D., Bozza, T., 2013. Non-redundant coding of aversive odours in the main olfactory pathway. Nature 497 (7450), 486–489.
Dong, Q., Du, L., Zhuang, L., Li, R., Liu, Q., Wang, P., 2013. A novel bioelectronic nose based on brain-machine interface using implanted electrode recording in vivo in olfactory bulb. Biosens. Bioelectron. 49, 263–269.
Dung, T.T., Oh, Y., Choi, S.J., Kim, I.D., Oh, M.K., Kim, M., 2018. Applications and advances in bioelectronic noses for odour sensing. Sensors 18 (1).
Ellis, H., Mulder, C., Valverde, E., Poling, A., Edwards, T., 2017. Reproducibility of African giant pouched rats detecting Mycobacterium tuberculosis. BMC Infect. Dis. 17 (1), 298.
Jezierski, T., Adamkiewicz, E., Walczak, M., Sobczyńska, M., Górecka-Bruzda, A., Ensminger, J., Papet, E., 2014. Efficacy of drug detection by fully-trained police dogs varies by breed, training level, type of drug and search environment. Forensic Sci. Int. 237, 112–118.
Kranz, W., Kitts, K., Strange, N., Cummins, J., Lotspeich, E., Goodpaster, J., 2014. On the smell of Composition C-4. Forensic Sci. Int. 236, 157–163.
Laurent, G., 2002. Olfactory network dynamics and the coding of multidimensional signals. Nat. Rev. Neurosci. 3, 884.
Leitch, O., Anderson, A., Kirkbride, K.P., Lennard, C., 2013. Biological organisms as volatile compound detectors: a review. Forensic Sci. Int. 232 (1–3), 92–103.
Lilly, J.M., 2017. Element analysis: a wavelet-based method for analysing time-localized events in noisy time series. Proc. Math. Phys. Eng. Sci. 473 (2200), 20160776.
McGann, J.P., Pirez, N., Gainey, M.A., Muratore, C., Elias, A.S., Wachowiak, M., 2005. Odorant representations are modulated by intra- but not interglomerular presynaptic inhibition of olfactory sensory neurons. Neuron 48 (6), 1039–1053.
Nakhleh, M.K., Amal, H., Jeries, R., Broza, Y.Y., Aboud, M., Gharra, A., Ivgi, H., Khatib, S., Badarneh, S., Har-Shai, L., Glass-Marmor, L., Lejbkowicz, I., Miller, A., Badarny, S., Winer, R., Finberg, J., Cohen-Kaminsky, S., Perros, F., Montani, D., Girerd, B., Garcia, G., Simonneau, G., Nakhoul, F., Baram, S., Salim, R., Hakim, M., Gruber, M., Ronen, O., Marshak, T., Doweck, I., Nativ, O., Bahouth, Z., Shi, D.Y., Zhang, W., Hua, Q.L., Pan, Y.Y., Tao, L., Liu, H., Karban, A., Koifman, E., Rainis, T., Skapars, R., Sivins, A., Ancans, G., Liepniece-Karele, I., Kikuste, I., Lasina, I., Tolmanis, I., Johnson, D., Millstone, S.Z., Fulton, J., Wells, J.W., Wilf, L.H., Humbert, M., Leja, M., Peled, N., Haick, H., 2017. Diagnosis and classification of 17 diseases from 1404 subjects via pattern analysis of exhaled molecules. ACS Nano 11 (1), 112–125.
Nardi-Agmon, I., Peled, N., 2017. Exhaled breath analysis for the early detection of lung cancer: recent developments and future prospects. Lung Canc. 8, 31–38.
Pedregosa, F., Varoquaux, G., Gramfort, A., Michel, V., Thirion, B., Grisel, O., Blondel, M., Prettenhofer, P., Weiss, R., Dubourg, V., Vanderplas, J., Passos, A., Cournapeau, D., Brucher, M., Perrot, M., Duchesnay, E., 2011. Scikit-learn: machine learning in Python. J. Mach. Learn. Res. 12, 2825–2830.
Pirez, N., Wachowiak, M., 2008. In vivo modulation of sensory input to the olfactory bulb by tonic and activity-dependent presynaptic inhibition of receptor neurons. J. Neurosci. 28 (25), 6360–6371.
Saha, D., Mehta, D., Altan, E., Chandak, R., Traner, M., Lo, R., Gupta, P., Singamaneni, S., Chakrabartty, S., Raman, B., 2020. Explosive sensing with insect-based biorobots. Biosens. Bioelectron. X 6, 100050.
Seo, I.S., Lee, H.G., Koo, B., Koh, C.S., Park, H.Y., Im, C., Shin, H.C., 2018. Cross detection for odor of metabolic waste between breast and colorectal cancer using canine olfaction. PloS One 13 (2), e0192629.
Smear, M., Resulaj, A., Zhang, J., Bozza, T., Rinberg, D., 2013. Multiple perceptible signals from a single olfactory glomerulus. Nat. Neurosci. 16 (11), 1687–1691.
Trivedi, D.K., Sinclair, E., Xu, Y., Sarkar, D., Walton-Doyle, C., Liscio, C., Banks, P., Milne, J., Silverdale, M., Kunath, T., Goodacre, R., Barran, P., 2019. Discovery of volatile biomarkers of Parkinson's disease from sebum. ACS Cent. Sci. 5 (4), 599–606.
Weiss, E., 2002. Selecting shelter dogs for service dog training. J. Appl. Anim. Welfare Sci. 5 (1), 43–62.
Wilson, C.D., Serrano, G.O., Koulakov, A.A., Rinberg, D., 2017. A primacy code for odor identity. Nat. Commun. 8 (1), 1477.